JACS
JOURNAL OF THE AMERICAN CHEMICAL SOCIETY
pubs.acs.org/JACS
Article

Enhanced Suppression of a Protein−Protein Interaction in Cells Using Small-Molecule Covalent Inhibitors Based on an *N*-Acyl-*N*-alkyl Sulfonamide Warhead

Tsuyoshi Ueda, Tomonori Tamura,* Masaharu Kawano, Keiya Shiono, Fruzsina Hobor, Andrew J. Wilson, and Itaru Hamachi*

Cite This: *J. Am. Chem. Soc.* 2021, 143, 4766−4774

ABSTRACT: Protein−protein interactions (PPIs) intimately govern various biological processes and disease states and therefore have been identified as attractive therapeutic targets for small-molecule drug discovery. However, the development of highly potent inhibitors for PPIs has proven to be extremely challenging with limited clinical success stories. Herein, we report irreversible inhibitors of the human double minute 2 (HDM2)/p53 PPI, which employ a reactive *N*-acyl-*N*-alkyl sulfonamide (NASA) group as a warhead. Mass-based analysis successfully revealed the kinetics of covalent inhibition and the modification sites on HDM2 to be the N-terminal α-amine and Tyr67, both rarely seen in traditional covalent inhibitors. Finally, we demonstrated prolonged p53-pathway activation and more effective induction of the p53-mediated cell death in comparison to a noncovalent inhibitor. This study highlights the potential of the NASA warhead as a versatile electrophile for the covalent inhibition of PPIs and opens new avenues for the rational design of potent covalent PPI inhibitors.

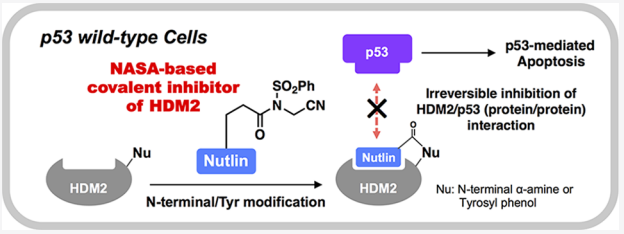

INTRODUCTION

Protein−protein interactions (PPIs) are key to all signaling pathways in cells. Thus, controlling PPIs with small molecules is an attractive therapeutic strategy for a wide range of diseases.[1,2] Although there are several successful examples such as Nutlin-3a[3] and its derivative Idasanutlin,[4,5] reversible inhibitors of a human double minute 2 (HDM2)/p53 PPI; the development of highly potent inhibitors for PPIs has been recognized as one of the most challenging tasks in drug discovery.[1,2] This arises because PPI interfaces are generally large (∼1000−2000 Å^2 per side) and shallow, making them less susceptible to high affinity and selective competitive inhibition with small-molecule ligands.[1,6] To overcome the unfavorable thermodynamics in blocking PPIs, the targeted covalent inhibition of PPIs has recently been considered as a promising strategy.[7] Targeted covalent inhibitors (TCIs) contain weakly electrophilic warheads in the protein ligand scaffold.[8] Upon ligand binding, TCIs can typically react with an amino acid side chain of the target protein as a consequence of the high effective molarity, reinforcing the noncovalent affinity and resulting in irreversible inhibition. Compared to noncovalent inhibitors, TCIs offer several advantages, including increased potency and prolonged duration of inhibition. To date, the design strategy for the established TCIs has focused on targeting cysteine residues near the ligand binding site because of its high reactivity toward modest electrophiles, such as acrylamides and chloroacetamides.[8−13] Unfortunately, however, PPI interfaces rarely contain free cysteine residues in an ideal position. Therefore, appropriate warheads that covalently target residues other than cysteine are highly desirable for the extension of the TCI approach to PPI inhibition.

Although still challenging, recent efforts identified several promising warheads for the rapid and selective covalent modification of noncysteine amino acids.[9−11,14] For example, aryl sulfonyl fluorides have been used for the covalent inhibition of PPIs targeting lysine, tyrosine, or histidine residues.[15] Our group also recently demonstrated that ligand-tethered *N*-acyl-*N*-alkyl sulfonamides (NASAs) efficiently react with the amino group of a noncatalytic lysine residue of Hsp90 and are applicable to the TCI approach.[16−18] This encouraged us that the NASA warhead would facilitate the development of effective TCIs for PPIs exploiting distinct reactivity.

Here, we report NASA-based small-molecule covalent inhibitors for the HDM2/p53 PPI, a promising therapeutic target for several types of cancers (Figure 1a).[3,19] While two covalent inhibitors based on stapled peptides for the HDM2/p53 PPI were recently reported, their modification sites, mechanisms of action, and target selectivity in a cellular context

Received: January 20, 2021
Published: March 18, 2021

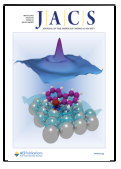

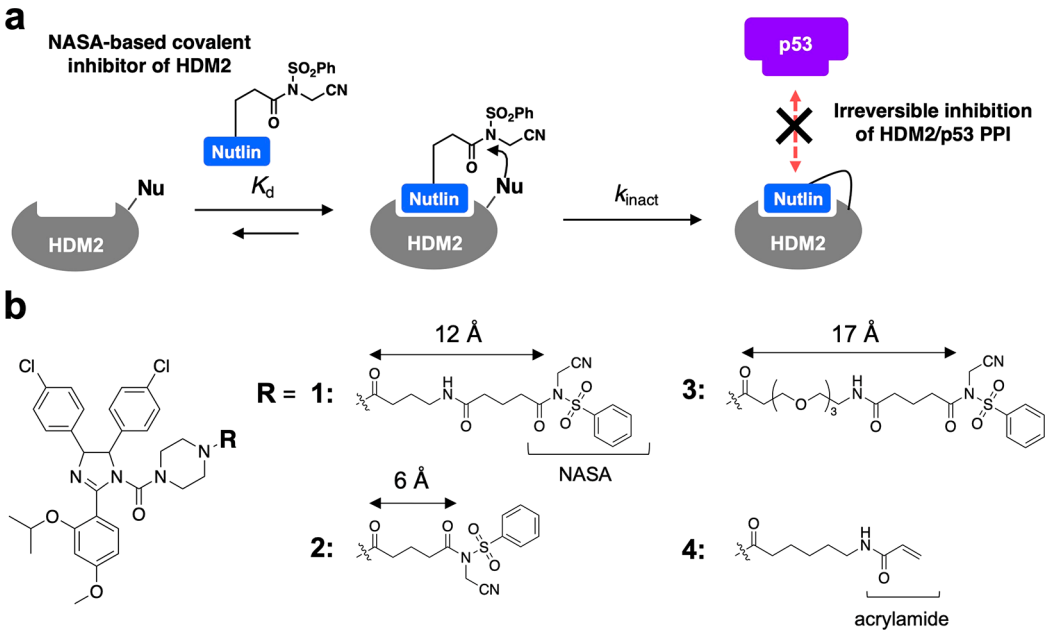

Figure 1. Irreversible inhibition of the HDM2/p53 PPI using NASA-appended Nutlin-3. (a) Schematic illustration of the reaction mechanism of the NASA-based covalent inhibitor. (b) Molecular structures of NASA-based covalent inhibitors **1**−**3** and acrylamide-based compound **4**.

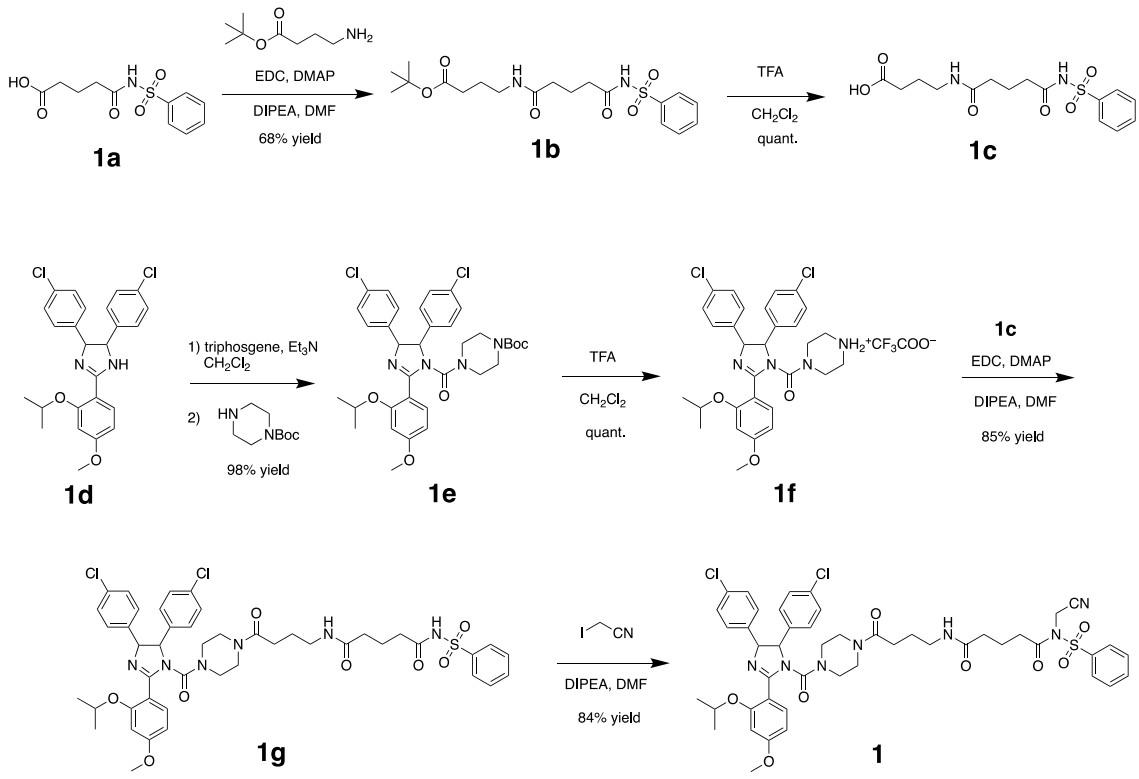

Figure 2. Synthesis scheme of covalent HDM2 inhibitor **1**.

were not fully evaluated.[20,21] In this work, we clearly showed that our optimal covalent inhibitor reacts with the N-terminal amino group and Tyr67 of HDM2 with rapid kinetics and selectively disrupts the HDM2/p53 interaction in an irreversible fashion in cells.

RESULTS AND DISCUSSION

Design and Synthesis of Covalent Inhibitors for HDM2. We employed (±)-Nutlin-3 (a mixture of Nutlin-3a and -3b, Figure S1),[3] a first-in-class reversible HDM2 inhibitor, as a scaffold for our covalent inhibitor because of its abundant information on structure−activity relationships and sufficient affinity (K_d = 0.263 × 10^{-6} M for the racemic mixture)[22] according to a guideline for the ligand-directed covalent modification of proteins with NASA chemistry.[16,17] The reported cocrystal structure of $HDM2_{17-108}$ with Nutlin-3a (the more potent enantiomer) (protein data bank (PDB): 4HG7) indicated to us that a targetable lysine (Lys51) for a

https://doi.org/10.1021/jacs.1c00703
J. Am. Chem. Soc. 2021, 143, 4766−4774

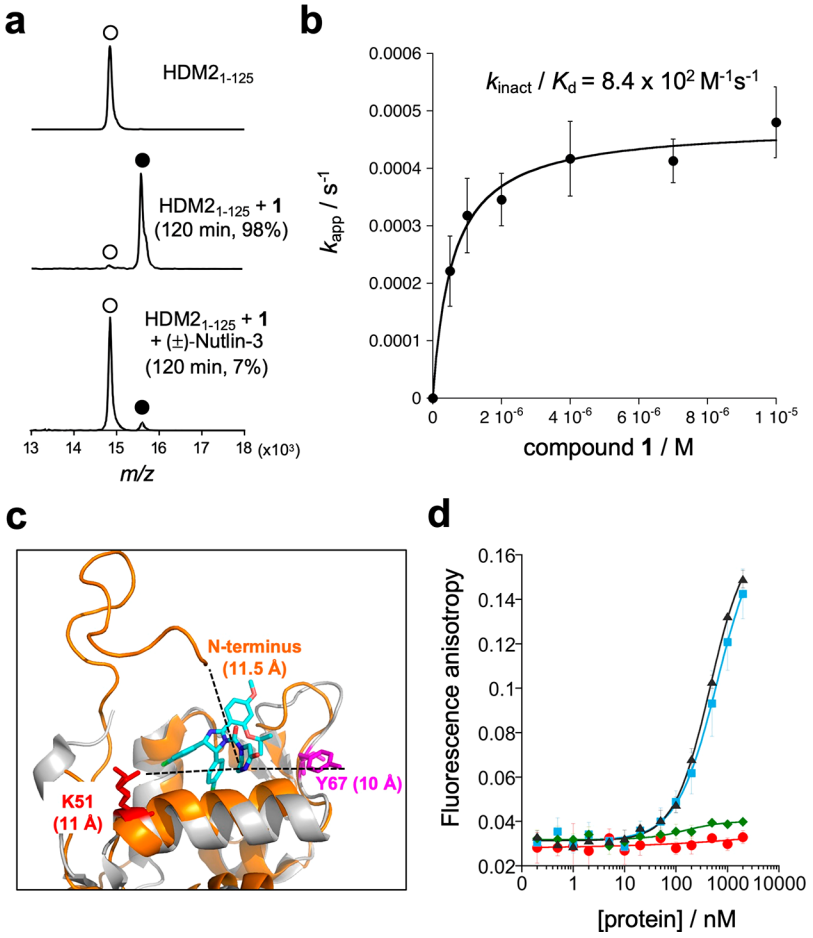

Figure 3. In vitro characterization of covalent HDM2 inhibition by **1**. (a) MALDI-TOF MS analysis of the covalent modification of the recombinant N-terminal domain of HDM2 (HDM2$_{1-125}$). Reaction conditions: 1 μM HDM2$_{1-125}$, 3 μM **1**, PBS buffer, pH 7.4, 37 °C. ○, native HDM2$_{1-125}$ (M_w = 14 955); ●, covalent adduct of the HDM2$_{1-125}$ with **1** (M_w = 15 703). (b) Kinetic analysis of the covalent modification of HDM2$_{1-125}$ with increasing concentrations of **1**. k_{app} was determined by the plots shown in Figure S4. Error bars represent the standard deviation, n = 3. (c) Superimposed model of the HDM2 (17−108 a.a.) (gray)−Nutlin-3a (cyan) complex (PDB: 4HG7) with HDM2 (1−118 a.a.) (orange; PDB: 1Z1M). (d) Fluorescence anisotropy changes in FL-labeled p53 peptide[28] (100 nM) upon addition of reversibly or irreversibly inhibited HDM2$_{1-125}$ (M1G) (0.2 to 2000 nM). Red ●, **1**-treated HDM2$_{1-125}$ (M1G) after SEC; blue ■, (±)-Nutlin-3-treated HDM2$_{1-125}$ (M1G) after SEC; green ♦, (±)-Nutlin-3-treated HDM2$_{1-125}$ (M1G) without SEC; ▲, nontreated HDM2$_{1-125}$ (M1G). Error bars represent the standard deviation, n = 3.

NASA warhead is located at a distance of approximately 11 Å from the 2-oxopiperazine moiety of Nutlin-3a (Figure S1). Therefore, we designed covalent HDM2 inhibitor **1** appended with a NASA group and an ∼12 Å linker (Figure 1b). The 2-oxopiperazine moiety of (±)-Nutlin-3 was replaced with a piperazine moiety to connect the NASA warhead. To examine structure−activity relationships, we also prepared inhibitors **2** and **3** containing a shorter (∼6 Å) and a longer (∼17 Å) linker, respectively, relative to **1** (Figure 1b). Acrylamide-type inhibitor **4** was also synthesized as a control compound that is mostly used for targeting cysteine. The synthesis of **1** was carried out as shown in Figure 2. The detailed procedures and synthesis of other compounds are described in the Supporting Information (SI). All of the final compounds were fully characterized by NMR and high-resolution mass spectrometry.

Characterization of the Covalent Modification of HDM2. We initially tested the covalent modification of HDM2 with **1**−**4** *in vitro*. Recombinant HDM2 N-terminal domain (1−125 a.a.) with an L33E mutation, for the improvement of protein stability, was obtained by a standard bacterial expression protocol (Figure S2). This protein (hereafter referred to as HDM2$_{1-125}$, 1 μM) was incubated with each covalent inhibitor (3 μM) at 37 °C in PBS buffer (pH 7.4). The matrix-assisted desorption/ionization time-of-flight mass spectrometry (MALDI-TOF MS) analysis of HDM2$_{1-125}$ treated with **1** and **3** gave a new peak corresponding to the addition of one molecule of the ligand moiety coupled with the loss of *N*-cyanomethylbenzenesulfonamide, and **2** afforded negligible conversion under this reaction condition (Figure 3a and Figure S3). It was also found that control compound **4** failed to modify the recombinant HDM2$_{1-125}$ (Figure S3). The time course analysis showed that the reaction with **1** and **3** is completed within 2 h, and the covalent modification was significantly suppressed in the presence of (±)-Nutlin-3 as a competitive ligand, indicating that the reaction was based on an affinity-mediated proximity effect (Figure S3).

As for compound **1**, we determined the affinity (K_d) and the rate constant of covalent modification (k_{inact}) using a previously reported MS-based method (Figure 3b and Figure S4).[16] The obtained K_d value of **1** was 5.7 × 10^{-7} M, which indicated that the incorporation of the linker and NASA warhead into the parent scaffold of (±)-Nutlin-3 (K_d = 0.263 × 10^{-6} M for a racemic mixture)[22] slightly reduced the binding affinity. The k_{inact} value of **1** was determined to be 4.8 × 10^{-4} s^{-1}. Then, the

https://doi.org/10.1021/jacs.1c00703
J. Am. Chem. Soc. 2021, 143, 4766−4774

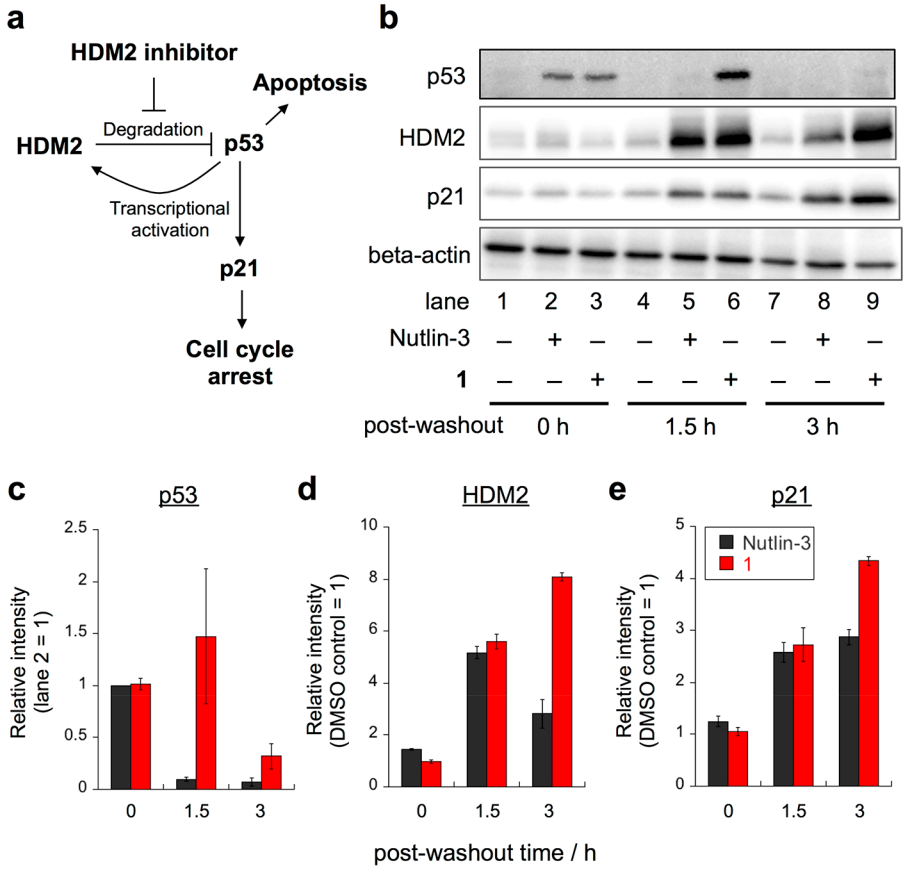

Figure 4. Evaluation of p53 activation in cells by irreversible HDM2 inhibition after compound washout. (a) Illustration of the HDM2/p53 pathway. (b) Western blotting analysis of p53 activation and up-regulation of HDM2 and p21. Cells were treated with (±)-Nutlin-3 or **1** for 1 h, followed by washing with media and further incubation for 1.5 or 3 h. Normalized band intensities of (c) p53, (d) HDM2, and (e) p21. Error bars represent the standard deviation, $n = 3$.

second-order rate constant k_{inact}/K_d value for **1** was estimated to be 8.4×10^2 M^{-1} s^{-1}, indicating that compound **1** would possess sufficient reactivity for effective covalent inhibition.

The modification sites on $HDM2_{1-125}$ after reaction with NASA-based covalent inhibitors were identified by MS-based peptide mapping analysis (Figure S5). Although **1** was designed to target Lys51, to our surprise the modification reaction occurred on the α-amino group of the N-terminus and Tyr67 of $HDM2_{1-125}$ (Figure S6). The N-terminal modification was also verified by top-down sequencing of $HDM2_{1-125}$ with in-source decay MALDI-TOF/TOF MS analysis (Figure S8). We also confirmed that **3** reacts with the N-terminal amine and Tyr67 as well as with **1** (Figures S5, S7, and S8). A Y67F mutation in $HDM2_{1-125}$ resulted in the disappearance of the corresponding Y67-labeled peptide with the remainder of the N-terminally labeled peptide in the peptide mapping analysis (Figures S9 and S10), which clearly indicated the modification of Tyr67.[23]

The N-terminal region of HDM2 is an intrinsically disordered region that modulates the function of HDM2, and it was truncated in the cocrystal structural analysis of the HDM2 (17−108 a.a.)/Nutlin-3 complex.[19] Indeed, the N-terminal region of HDM2 has rarely been observed[24] in cocrystal structures, and the first five residues were never crystallographically resolved.[19] We thus made a superimposed model of the HDM2 (17−108 a.a.)/Nutlin-3a complex (PDB: 4HG7) with HDM2 (1−118 a.a.) (PDB: 1Z1M) determined by an NMR study and confirmed that the N-terminal amino group is likely located in the vicinity of Nutlin-3a (within ∼12 Å) (Figure 3c). While Lys51 is also positioned in proximity to the ligand, the lower pK_a value of the N-terminal α-amino group ($pK_a \approx 8$) compared to the ε-amino group of a Lys side chain ($pK_a \approx 10$) may contribute to the regioselectivity of the reaction with the NASA warhead.[25,26] The modification on Tyr67 is also reasonable, given its distance from Nutlin-3a (∼10 Å) (Figure 3c) and our recent study on the amino acid selectivity of the NASA warhead.[27]

The reaction of NASA-tethered covalent inhibitors toward the N-terminus and Tyr67 was also evaluated in live HEK293T cells transiently expressing $HDM2_{1-125}$ or its variants with probes **5**−**7** equipped with a clickable alkyne tag in the (±)-Nutlin-3 scaffold of **1**−**3**, respectively. (See Figure S11 for their molecular structures and reaction profiles with $HDM2_{1-125}$.) The cell-based evaluation of modification sites with **5** and **7** was consistent with *in vitro* experiments using **1** and **3**, respectively, that is, these modified the N-terminus and Tyr67 (Figure S12). On the other hand, unlike the case of *in vitro* reaction, short linker type compound **6** (an analog of **2**) can covalently bind to the HDM2 N-terminal domain in the live cell context, and the modification site is exclusively the N-terminus. (See the Figure S12 caption for a more detailed discussion.) Although these results suggest that **2** and **3** are also promising for the covalent inhibition of HDM2, they showed serious p53-independent cytotoxicity (Figure S13) while **1** did not. Since this study focuses on the development of covalent inhibitors capable of blocking HDM2−p53 interaction and the evaluation of how efficient these are for selectively activating the p53

https://doi.org/10.1021/jacs.1c00703
J. Am. Chem. Soc. 2021, 143, 4766−4774

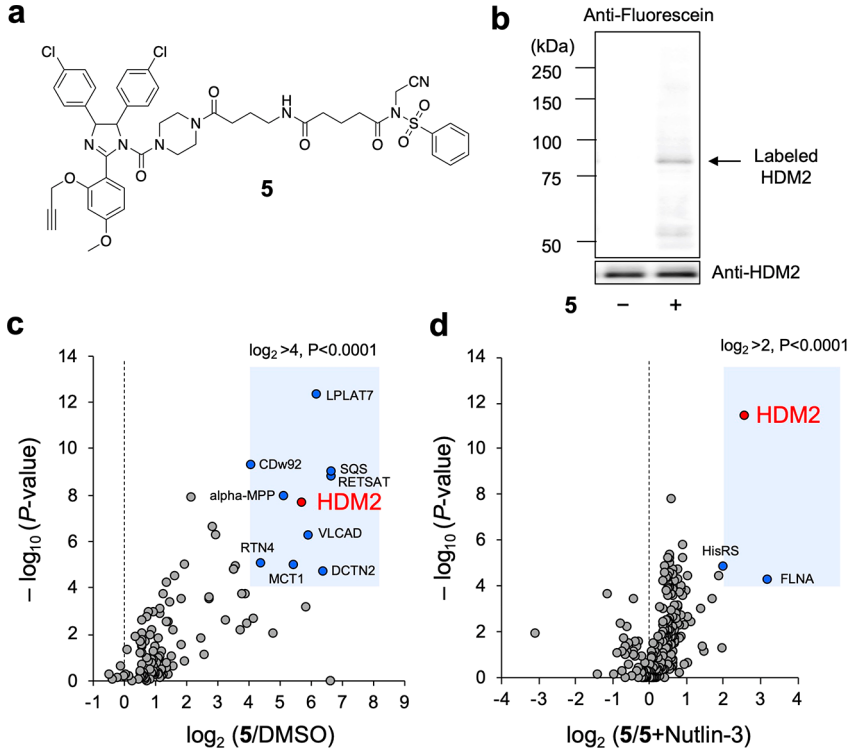

Figure 5. Evaluation of intracellular selectivity of NASA-based HDM2 covalent inhibitor. (a) Molecular structure of compound **5**. (b) Western blotting analysis of the labeling reaction with **5** (0.3 μM, 1 h) in live SJSA1 cells. After labeling, the labeled proteins were modified with fluorescein-azide via click chemistry, followed by Western blotting using antifluorescein antibody (also see the Supporting Information). Volcano plots display proteins enriched with neutravidin beads after clicking a desthiobiotin tag for proteins labeled with **5** relative to (c) DMSO control or (d) a competitive condition with (±)-Nutlin-3. The protein groups with $P < 0.0001$ and $\log_2$(**5**/DMSO) > 4 or $\log_2$(**5**/**5**+(±)-Nutlin-3) > 2 are highlighted in blue in (c) and (d), respectively. A plot indicating HDM2 is colored red. $n = 3$; P is the Benjamini−Hochberg adjusted P value. All proteins identified in this study are listed in Supporting Information Supplementary Data 1.

pathway in live cells, we determined to use **1** for a more detailed investigation in the following study.

Inhibition of HDM2/p53 Interaction In Vitro. Next, we attempted to confirm whether **1** can irreversibly inhibit the HDM2/p53 interaction with size exclusion chromatography (SEC)-based fluorescence anisotropy analysis. In this study, we used a more stable $HDM2_{1-125}$ M1G mutant since the original $HDM2_{1-125}$ is too unstable to be used for this analysis (See Figures S2 and S14−S17 for the primary structure of $HDM2_{1-125}$ (M1G), the reaction with **1**, and the modification sites.) **1**- and (±)-Nutlin-3-treated $HDM2_{1-125}$ (M1G) were subjected to SEC and subsequently used in fluorescence anisotropy measurements with the fluorescently labeled p53 peptide.[28] The addition of **1**-modified $HDM2_{1-125}$ (M1G) (~90% modification yield) to the peptide did not change the anisotropy, indicating that the p53 peptide was incapable of binding to the p53 binding cleft on $HDM2_{1-125}$ (M1G) due to occupancy by the covalently bound **1** on the interaction surface even after the purification by SEC (red line in Figure 3d). Similarly, no anisotropy change was observed in the mixture of $HDM2_{1-125}$ (M1G) and (±)-Nutlin-3 without SEC purification (green line). In sharp contrast, after SEC purification of the mixture of $HDM2_{1-125}$ (M1G) and (±)-Nutlin-3, a concentration-dependent response of the anisotropy was observed similar to that which was observed using apo-$HDM2_{1-125}$ (M1G), indicating that (±)-Nutlin-3 was removed from the ligand-binding site of $HDM2_{1-125}$ (M1G) by dilution during SEC purification (blue and black lines). Taken together, these results clearly indicated that covalent inhibitor **1** has a prolonged residence time on HDM2 and thereby shows increased HDM2/p53 inhibitory potency under dilute conditions, in comparison to noncovalent inhibitor (±)-Nutlin-3.

Activation of the p53 Pathway by Covalent HDM2 Inhibitor 1 in Living Cells. The cellular potency and durability of **1** were examined with osteosarcoma SJSA1 cells expressing wild-type p53.[29] Ubiquitin E3 ligase HDM2 is overexpressed in many different cancer cell lines and promotes the degradation of tumor suppressor p53 through binding its transactivation domain. Inhibition of the HDM2/p53 PPI can restore p53 expression levels, leading to the transcriptional induction of p53-regulated proteins (including HDM2 and p21), cell cycle arrest, and apoptosis (Figure 4a).[3,19,30] We first assessed the impact of **1** on the expression levels of p53, HDM2, and p21 by Western blotting analysis. SJSA1 cells were incubated with (±)-Nutlin-3 or **1** for 1 h and then washed and incubated for another 1.5 or 3 h. (±)-Nutlin-3 and **1** caused an increase in the levels of p53 before washing the cells (Figures 4b,c, S18, and S19), indicating the inhibition of the HDM2/p53 PPI in both cases. On the other hand, 1.5 h after washing, the p53 signal had almost disappeared in (±)-Nutlin-3-treated cells due to washout of the reversibly bound inhibitor, whereas it was still clearly detected in **1**-treated cells (Figure 4c). This explicitly indicates the irreversible and sustained inhibition of the HDM2/p53 PPI with **1**. Three hours after washing, the p53 signal was significantly reduced even in cells treated with **1**. Presumably this arises because the expression of nascent HDM2 was induced by the activated p53 pathway.[3] Indeed, we confirmed the up-regulation of HDM2 and p21 in the cells treated with both (±)-Nutlin-3 and

https://doi.org/10.1021/jacs.1c00703
J. Am. Chem. Soc. 2021, 143, 4766−4774

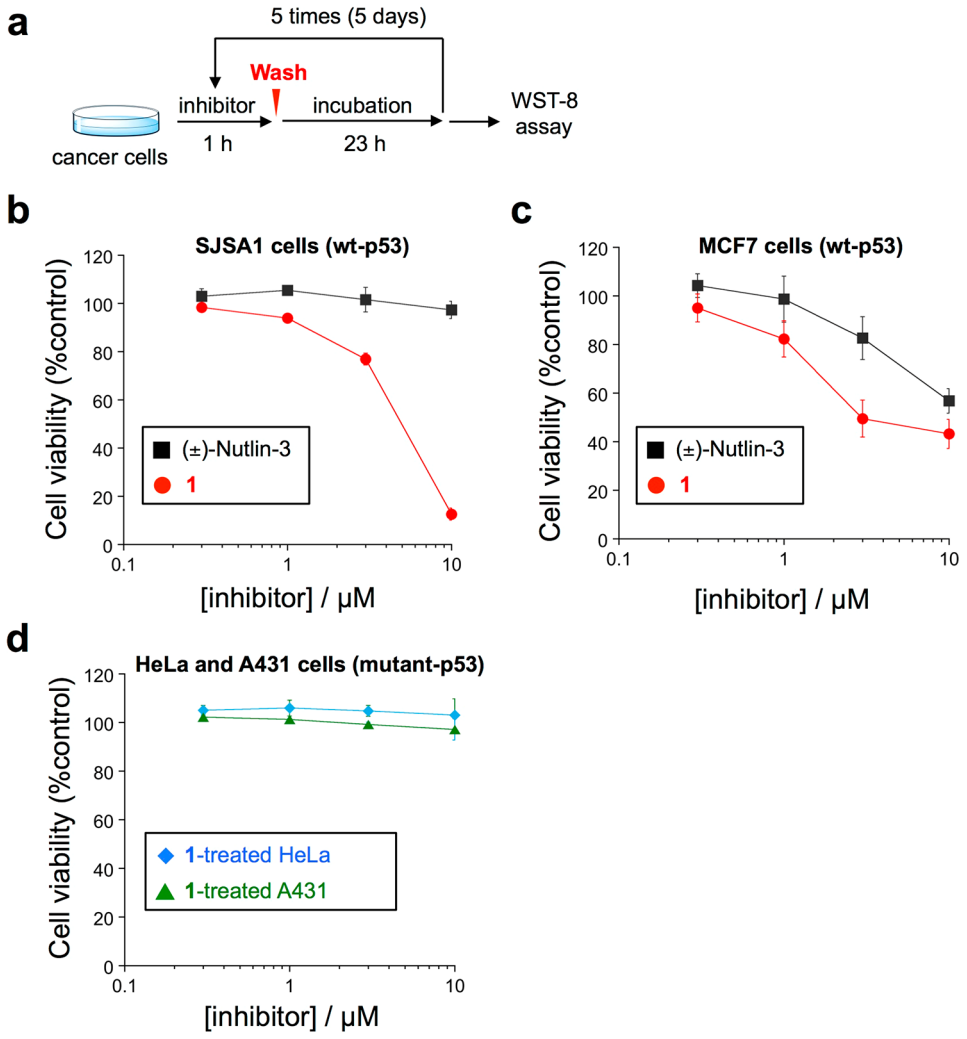

Figure 6. Effect of covalent inhibitor **1** on the growth and viability of cultured cancer cells. (a) Schematic workflow of the cell viability assay under a repetitive washout condition. (b–d) Viability of (b) SJSA1, (c) MCF7, and (d) HeLa or A431 cells after repetitive treatments of (±)-Nutlin-3 or **1** under the washout condition. Error bars represent the standard error of the mean, $n = 4$.

1 at the 1.5 and 3 h time points (Figure 4d,e). Note that **1** caused a longer-term and more potent elevation in the level of HDM2 and p21 proteins, compared to (±)-Nutlin-3,[31] highlighting the potential advantages of covalent inhibitor **1** under washout conditions.

Evaluation of the Target Selectivity of the NASA-Based Covalent HDM2 Inhibitor. We subsequently evaluated the cellular target engagement of the NASA-based covalent inhibitor using probe **5** (Figure 5a; the reaction with recombinant $HDM2_{1-125}$ is shown in Figure S11). SJSA1 cells were incubated with **5** (0.3 μM, 1 h), and probe-labeled proteins were detected by Western blotting with an antifluorescein antibody after the copper-catalyzed conjugation of fluorescein-azide.[32] A 90 kDa band was clearly observed in the blotting analysis (Figure 5b) and identified as the labeled HDM2 by a pull-down assay (Figure S20), revealing the selective labeling of endogenous HDM2 with **5**. Coincubation of **1** in the reaction with **5** prohibited the labeling of HDM2, which demonstrated that **1** binds to the p53 binding pocket of HDM2 inside cells (Figure S21). The proteome-wide targets of **5** in SJSA1 cells were also evaluated by a SILAC (stable isotope labeling by amino acids in cell culture)-based quantitative chemoproteomics method (Figure S22).[33] Ten proteins including HDM2 were identified as proteins significantly reacting with **5** ($\log_2$(**5**/DMSO) > 4, $P < 0.0001$), and HDM2 was characterized as the protein strongly competing by (±)-Nutlin-3 (Figure 5c,d, Supporting Information Supplementary Data 1). Thus, both Western blotting analysis and chemoproteomic data clearly revealed that the NASA-based HDM2 inhibitor reacts with intracellular HDM2 with sufficient selectivity to irreversibly inhibit its activity.

Cytotoxic Effect of the Covalent HDM2 Inhibitor under Washout Conditions. Finally, the effect of covalent inhibitor **1** on cell viability was examined. Four cell lines, two with wild-type (SJSA1 and MCF7) and two with mutant p53 (HeLa and A431), were tested.[34] In this experiment, cells were transiently incubated with inhibitors for 1 h, followed by washing and further incubation for 23 h without inhibitors. This procedure was repeated five times, and then the cell viability was evaluated with a WST-8 assay (Figure 6a).[35] Covalent inhibitor **1** clearly showed antiproliferative and cytotoxic activity for p53 wild-type SJSA1 and MCF7 cells at a concentration of 1–10 μM (red circle plot in Figure 6b,c), whereas the treatment of (±)-Nutlin-3 was less efficient under this rigorous washout condition (black squares in plot). Unlike cells expressing wild-type p53 (SJSA1 and MCF7), HeLa and A431 cells bearing

https://doi.org/10.1021/jacs.1c00703
J. Am. Chem. Soc. 2021, 143, 4766–4774

inactive mutant p53 were not susceptible to **1** (blue and green plots in Figure 6d, respectively). These results revealed that **1** selectively induced p53 pathway-dependent cell apoptosis via the covalent inhibition of HDM2 without nonspecific cytotoxicity arising from the NASA warhead.

CONCLUSIONS

We have demonstrated that an HDM2 inhibitor equipped with a NASA warhead (compound **1**) irreversibly suppresses the HDM2/p53 PPI both *in vitro* and in living cells. To our knowledge, the present study is the first report of a small-molecule-based covalent inhibitor of HDM2. Notably, in addition to lysine, which we identified previously,[16] an N-terminal α-amine and tyrosine in the protein were identified to be targetable with the NASA warhead for the first time.[27] The N-terminal modification may offer a unique advantage that is unlikely affected by point-mutation-mediated drug resistance, often reported in recent covalent drug development programs.[36] Furthermore, the tyrosine on the protein surface is still challenging to rationally target using current TCI chemistries in spite of a few examples of tyrosine-targeting covalent inhibitors with sulfur−fluoride or −triazole exchange (SuFEx/SuTEx) chemistry;[15,37−39] therefore, our results expand the breadth of labeling chemistry that can be exploited in TCI. Thus, the results of this study not only demonstrate the high potential of the NASA warhead as a versatile electrophile for the covalent inhibition of PPIs but also provide valuable insights for the design strategy of new TCIs.

In general, it may be considered that proteins which undergo rapid turnover, such as HDM2 (<30 min), are not suitable targets for irreversible inhibition. Nevertheless, this work has demonstrated that the irreversible inhibition of HDM2, in comparison to reversible inhibition, results in prolonged activation of p53 and stronger induction of its transcriptional targets. The role of HDM2 as a negative regulator of p53 presents challenges in terms of a therapeutic window,[19,30] hence these results uncover an approach to address this challenge. More broadly, the results highlight that opportunities for intervention in biological systems might arise through greater understanding and control over the time frame of the biological process as evidenced by the differential effects on protein levels that are observed for covalent and noncovalent inhibitors. Although further mechanistic investigation is required, this suggests to us that a covalent inhibition strategy may represent a powerful approach to enhancing drug efficacy for short-lived proteins and will broaden the scope of the TCI approach targeting PPIs.

EXPERIMENTAL SECTION

Synthesis. All synthesis procedures and compound characterizations are described in the Supporting Information.

Preparation of the Recombinant HDM2 N-Terminal Domain. The recombinant HDM2 N-terminal domain was obtained by bacterial expression as a fusion protein with a His10 tag and a TEV protease cleavage site at its N- or C-terminus (also see Figure S2). The pET28a-HDM2 plasmid encoding HDM2 (17−125 a.a., with an L33E mutation to improve the protein stability) was amplified by PCR with the 5′-primer (5′-aaccgatggcgcagtgaccacctcacagattccagcttcg-3′) and the 3′-primer (5′-ggaactgacatgttggtgttgcatccctggaagtacag-3′) to insert the 1−16 sequence of HDM2 with a TEV site and ligated with the KLD enzyme mixture (New England Biolabs) to yield pET28a-HDM2$_{1-125}$ (M1G). pET28a-HDM2$_{1-125}$ was constructed by a two-step procedure. First, the N-terminal His10 tag−TEV site of the pET28a-HDM2$_{1-125}$ (M1G) was deleted and N-terminal methionine was introduced by PCR with the 5′-primer (5′- tgcaacaccaacatgtcag-3′) and the 3′-primer (5′-catggtatatctccttcttaaag-3′), and then the tag sequence was inserted into the C-terminal region by PCR with the 5′-primer (5′-tcatcatcatcatcatcatcactagctcgagcaccaccac-3′) and the 3′-primer (5′-tgatgtccctggaagtacaggttttcgttctcactcacagatgtacctg-3′). Using the pET28a-HDM2$_{1-125}$ as a template, a Y67F mutation was introduced with a Q5 site-directed mutagenesis kit (New England Biolabs) with the 5′-primer (5′-taaacgattattcgatgagaagcaacaac-3′) and the 3′-primer (5′-gtcataatatactggccaag-3′). The PCR amplified sequences were verified by DNA sequencing. The expression vectors were transformed into *Escherichia coli* BL21 (DE3) or Rosetta (DE3) (Merck). The cells were grown in LB media containing kanamycin at 37 °C to an optical density (600 nm) of 0.6, at which time the expression of the fusion protein was induced by the addition of 1 mM IPTG. After growth for an additional 23 h at 18 °C, the cells were harvested by centrifugation. The cell pellets were resuspended in a mixture of 50 mM Tris-HCl, 500 mM NaCl, and 10% glycerol at pH 7.5 and were then lysed by sonication. The proteins were purified from the soluble fraction of the lysate using a TALON metal affinity resin (Clontech) and dialyzed against a mixture of 50 mM HEPES, 0.5 mM EDTA, and 1 mM DTT at pH 7.0. The His tag in the fusion protein was cleaved with ProTEV plus (Promega) at 30 °C for 2−8 h and then dialyzed against phosphate-buffered saline (PBS). The resulting (tag-free) protein was purified by passing it through a TALON metal affinity resin. The concentrations of the obtained HDM2 N-terminal domain were determined with a BCA assay (Pierce).

Modification of HDM2 In Vitro. Purified HDM2$_{1-125}$ (1 μM) was incubated with reagent (3 μM) in PBS buffer (pH 7.4) at 37 °C. Aliquots at different time points were taken and then desalted using a Ziptip-C4 (Merck), and the modification yields were determined by MALDI-TOF MS (matrix: CHCA).

Peptide Mapping of the Modified N-Terminal Domain of HDM2. The modified HDM2$_{1-125}$ (2.7−5 μM) was mixed with ProteaseMAX (Promega, at a final concentration of 0.05%) and Trypsin/Lys-C mix (Promega, 2 μg). After incubation at 37 °C for 16 h, the digested peptides were desalted with a Ziptip-C18 and analyzed by MALDI-TOF/TOF MS (Bruker Daltonics, UltrafleXtreme) (matrix: CHCA). The mass scan range was m/z 500−5000 or 1000−5000, and the laser intensity was set to be 50−60%. The raw MS data files were analyzed by FlexAnalysis 3.4 (Bruker) to create peak lists based on the recorded spectra. The mass peaks assigned as the modified peptide were selected and subjected to MS/MS analysis in LIFT mode with a precursor mass tolerance and a fragment ion mass tolerance of 0.5 Da. Cysteine carbamidomethylation was set as a fixed modification. Methionine oxidation was allowed as a variable modification. The MS/MS spectra were analyzed by the Biotools and Sequence editor (Bruker).

In-Source Decay MALDI-TOF/TOF MS Analysis. The modified HDM2$_{1-125}$ (1−5 μM) was desalted by a Ziptip-C4 and spotted on a MALDI-TOF MS plate. The protein sample was subjected to strong laser irradiation (~100% laser intensity) with UltrafleXtreme, and the m/z range of 100−2000 was measured. The raw MS data files were analyzed by FlexAnalysis 3.4 to create peak lists based on the recorded spectra. For MS/MS analysis, the mass peaks corresponding to the modified Met or Met-Cys were selected and analyzed by the LIFT mode.

Fluorescence Anisotropy Measurement to Evaluate the HDM2/p53 Interaction. The **1**-modified or (±)-Nutlin3-treated HDM2$_{1-125}$ (M1G) was subjected to size exclusion chromatography (TOYOPEARL HW-40F column) with PBS buffer (pH 7.4). To a solution of fluorescein-labeled p53 peptide (100 nM) (Ac-SQETFS-DLWKLLPENNVC(Flu)-NH$_2$)[28] in PBS buffer (pH 7.4, 0.02 mg/mL BSA), the protein solution was added. The fluorescence anisotropy measurements were performed by using a PerkinElmer LS-55 luminescence spectrometer.

Western Blotting Analysis of p53 Activation by Covalent Inhibition. SJSA1 cells (2×10^5 cells) were seeded on a six-well plate (Corning) and incubated in RPMI-1640 supplemented with 10% fetal bovine serum (FBS, Gibco), penicillin (100 units/mL), streptomycin (100 mg/mL), and amphotericin B (250 ng/mL) for 48 h at 37 °C under 5% CO_2. After washing twice with HEPES-modified RPMI-1640

https://doi.org/10.1021/jacs.1c00703
J. Am. Chem. Soc. 2021, 143, 4766−4774

(FBS-free) medium, the cells were incubated in the medium containing (±)-Nutlin-3 (10 μM) or **1** (10 μM) for 1 h at 37 °C. The cells were washed twice with RPMI-1640 supplemented with 10% FBS and further incubated for 1.5 or 3 h. The cells were washed with PBS and lysed with RIPA buffer (pH 7.4, 25 mM Tris−HCl, 150 mM NaCl, 0.1% SDS, 1% Nonidet P-40, 0.25% deoxycholic acid) containing 1% protease inhibitor cocktail set III (Calbiochem). The lysed samples were centrifuged (15 200*g*, 10 min at 4 °C). The protein concentrations of the supernatant were analyzed by BCA assay, and the normalized lysates were mixed with 1/4 volume of 5 × sample buffer (pH 6.8, 312.5 mM Tris−HCl, 25% sucrose, 10% SDS, 0.025% bromophenol blue) containing 250 mM DTT and vortex mixed for 1 h at room temperature. The samples were subjected to Western blotting analysis using anti-p53 (CST, no. 2527), MDM2/HDM2 (CST, no. 86934), p21 (CST, no. 2947), beta actin (Abcam, ab8226), antirabbit IgG-HRP conjugate (CST, no. 7074S), and antimouse IgG-HRP conjugate (CST, no. 7076S) antibodies.

Cell Viability Assay. SJSA1 cells (4×10^4 cells), MCF7 cells (4×10^4 cells), HeLa cells (2×10^4 cells), or A431 cells (2×10^4 cells) were seeded on a 24-well plate and incubated in RPMI-1640 (for SJSA1) or DMEM (for MCF7, HeLa and A431) supplemented with 10% FBS, penicillin (100 units/mL), streptomycin (100 mg/mL), and amphotericin B (250 ng/mL) for 24−48 h at 37 °C under 5% CO_2. After washing twice with HEPES-modified RPMI-1640 or DMEM (FBS-free) medium, the cells were incubated in the medium containing (±)-Nutlin-3 or covalent inhibitor (0.3−10 μM) for 1 h at 37 °C. The cells were washed twice with culture medium and further incubated for 23 h. This procedure was repeated five times. The cell viability was assessed using Cell Counting Kit-8 (Dojin). The absorbance of each well was measured at 450 nm with infinite M200 (TECAN).

■ ASSOCIATED CONTENT

Supporting Information

The Supporting Information is available free of charge at https://pubs.acs.org/doi/10.1021/jacs.1c00703.

Figures S1−S56, procedures of biological experiments, synthetic procedures, and compound characterization (PDF)

Supplementary Data 1 (XLSX)

■ AUTHOR INFORMATION

Corresponding Authors

Tomonori Tamura − *Department of Synthetic Chemistry and Biological Chemistry, Graduate School of Engineering, Kyoto University, Kyoto 615-8510, Japan;* orcid.org/0000-0003-1648-9296; Email: tamura@sbchem.kyoto-u.ac.jp

Itaru Hamachi − *Department of Synthetic Chemistry and Biological Chemistry, Graduate School of Engineering, Kyoto University, Kyoto 615-8510, Japan; ERATO (Exploratory Research for Advanced Technology, JST), Tokyo 102-0075, Japan;* orcid.org/0000-0002-3327-3916; Email: ihamachi@sbchem.kyoto-u.ac.jp

Authors

Tsuyoshi Ueda − *Department of Synthetic Chemistry and Biological Chemistry, Graduate School of Engineering, Kyoto University, Kyoto 615-8510, Japan*

Masaharu Kawano − *Department of Synthetic Chemistry and Biological Chemistry, Graduate School of Engineering, Kyoto University, Kyoto 615-8510, Japan*

Keiya Shiono − *Department of Synthetic Chemistry and Biological Chemistry, Graduate School of Engineering, Kyoto University, Kyoto 615-8510, Japan*

Fruzsina Hobor − *School of Chemistry and Astbury Centre for Structural Molecular Biology, University of Leeds, Leeds LS2 9JT, United Kingdom*

Andrew J. Wilson − *School of Chemistry and Astbury Centre for Structural Molecular Biology, University of Leeds, Leeds LS2 9JT, United Kingdom;* orcid.org/0000-0001-9852-6366

Complete contact information is available at: https://pubs.acs.org/10.1021/jacs.1c00703

Notes

The authors declare no competing financial interest.

■ ACKNOWLEDGMENTS

We thank Eriko Kusaka (Kyoto University) for experimental support of the NMR measurements. We also thank Dr. Muneo Tsujikawa for plasmid construction. This work was funded by a Research Fellowship from the Japan Society for the Promotion of Science (JSPS) for Young Scientists to T.U., a Grant-in-Aid for Young Scientists (18K14334), and a Grant-in-Aid for Scientific Research on Innovative Areas "Integrated Bio-metal Science" (19H05764) to T.T., and Japan Science and Technology Agency (JST) ERATO grant JPMJER1802 to I.H. This work was also supported by a Grant-in-Aid for Scientific Research on Innovative Areas "Chemistry for Multimolecular Crowding Biosystems" (17H06348), EPSRC (EP/N013573/1). A.J.W. holds a Royal Society Leverhulme Trust Senior Fellowship (SRF/R1/191087). The MS raw data and analysis files have been deposited in the ProteomeXchange Consortium (http://proteomecentral.proteomexchange.org) via the jPOST partner repository (http://jpostdb.org)[40] with data set identifier PXD018105.

■ REFERENCES

(1) Arkin, M. R.; Tang, Y.; Wells, J. A. Small-Molecule Inhibitors of Protein-Protein Interactions: Progressing toward the Reality. *Chem. Biol.* **2014**, *21*, 1102−1114.

(2) Mabonga, L.; Kappo, A. P. Protein-Protein Interaction Modulators: Advances, Successes and Remaining Challenges. *Biophys. Rev.* **2019**, *11*, 559−581.

(3) Vassilev, L. T.; Vu, B. T.; Craves, B.; Carvajal, D.; Podlaski, F.; Filipovic, Z.; Kong, N.; Kammlott, U.; Lukacs, C.; Klein, C.; Fotouhi, N.; Liu, E. A. In Vivo Activation of the P53 Pathway by Small-Molecule Antagonists of MDM2. *Science* **2004**, *303*, 844−848.

(4) Montesinos, P.; Beckermann, B. M.; Catalani, O.; Esteve, J.; Gamel, K.; Konopleva, M. Y.; Martinelli, G.; Monnet, A.; Papayannidis, C.; Park, A.; Récher, C.; Rodríguez-Veiga, R.; Röllig, C.; Vey, N.; Wei, A. H.; Yoon, S. S.; Fenaux, P. MIRROS: A Randomized, Placebo-Controlled, Phase III Trial of Cytarabine ± Idasanutlin in Relapsed or Refractory Acute Myeloid Leukemia. *Future Oncol.* **2020**, *16*, 807−815.

(5) Ding, Q.; Zhang, Z.; Liu, J. J.; Jiang, N.; Zhang, J.; Ross, T. M.; Chu, X. J.; Bartkovitz, D.; Podlaski, F.; Janson, C.; Tovar, C.; Filipovic, Z. M.; Higgins, B.; Glenn, K.; Packman, K.; Vassilev, L. T.; Graves, B. Discovery of RG7388, a Potent and Selective P53-MDM2 Inhibitor in Clinical Development. *J. Med. Chem.* **2013**, *56*, 5979−5983.

(6) Hwang, H.; Vreven, T.; Janin, J.; Weng, Z. Protein-protein docking benchmark version 4.0. *Proteins: Struct., Funct., Genet.* **2010**, *78*, 3111−3114.

(7) Way, J. C. Covalent Modification as a Strategy to Block Protein-Protein Interactions with Small-Molecule Drugs. *Curr. Opin. Chem. Biol.* **2000**, *4*, 40−46.

(8) Baillie, T. A. Targeted Covalent Inhibitors for Drug Design. *Angew. Chem., Int. Ed.* **2016**, *55*, 13408−13421.

(9) Gehringer, M.; Laufer, S. A. Emerging and Re-Emerging Warheads for Targeted Covalent Inhibitors: Applications in Medicinal Chemistry and Chemical Biology. *J. Med. Chem.* **2019**, *62*, 5673−5724.

(10) Lonsdale, R.; Ward, R. A. Structure-Based Design of Targeted Covalent Inhibitors. *Chem. Soc. Rev.* **2018**, *47*, 3816−3830.
(11) Zhang, T.; Hatcher, J. M.; Teng, M.; Gray, N. S.; Kostic, M. Recent Advances in Selective and Irreversible Covalent Ligand Development and Validation. *Cell Chem. Biol.* **2019**, *26*, 1486−1500.
(12) Shindo, N.; Fuchida, H.; Sato, M.; Watari, K.; Shibata, T.; Kuwata, K.; Miura, C.; Okamoto, K.; Hatsuyama, Y.; Tokunaga, K.; Sakamoto, S.; Morimoto, S.; Abe, Y.; Shiroishi, M.; Caaveiro, J. M. M.; Ueda, T.; Tamura, T.; Matsunaga, N.; Nakao, T.; Koyanagi, S.; Ohdo, S.; Yamaguchi, Y.; Hamachi, I.; Ono, M.; Ojida, A. Selective and Reversible Modification of Kinase Cysteines with Chlorofluoroacetamides. *Nat. Chem. Biol.* **2019**, *15*, 250−258.
(13) Tokunaga, K.; Sato, M.; Kuwata, K.; Miura, C.; Fuchida, H.; Matsunaga, N.; Koyanagi, S.; Ohdo, S.; Shindo, N.; Ojida, A. Bicyclobutane Carboxylic Amide as a Cysteine-Directed Strained Electrophile for Selective Targeting of Proteins. *J. Am. Chem. Soc.* **2020**, *142*, 18522−18531.
(14) Cuesta, A.; Wan, X.; Burlingame, A. L.; Taunton, J. Ligand Conformational Bias Drives Enantioselective Modification of a Surface-Exposed Lysine on Hsp90. *J. Am. Chem. Soc.* **2020**, *142*, 3392−3400.
(15) Gambini, L.; Baggio, C.; Udompholkul, P.; Jossart, J.; Salem, A. F.; Perry, J. J. P.; Pellecchia, M. Covalent Inhibitors of Protein-Protein Interactions Targeting Lysine, Tyrosine, or Histidine Residues. *J. Med. Chem.* **2019**, *62*, 5616−5627.
(16) Tamura, T.; Ueda, T.; Goto, T.; Tsukidate, T.; Shapira, Y.; Nishikawa, Y.; Fujisawa, A.; Hamachi, I. Rapid Labelling and Covalent Inhibition of Intracellular Native Proteins Using Ligand-Directed N-Acyl-N-Alkyl Sulfonamide. *Nat. Commun.* **2018**, *9*, 1870.
(17) Tamura, T.; Hamachi, I. Chemistry for Covalent Modification of Endogenous/Native Proteins: From Test Tubes to Complex Biological Systems. *J. Am. Chem. Soc.* **2019**, *141*, 2782−2799.
(18) Ueda, T.; Tamura, T.; Hamachi, I. Development of a Cell-Based Ligand-Screening System for Identifying Hsp90 Inhibitors. *Biochemistry* **2020**, *59*, 179−182.
(19) Khoo, K. H.; Verma, C. S.; Lane, D. P. Drugging the P53 Pathway: Understanding the Route to Clinical Efficacy. *Nat. Rev. Drug Discovery* **2014**, *13*, 217−236.
(20) Hoppmann, C.; Wang, L. Proximity-Enabled Bioreactivity to Generate Covalent Peptide Inhibitors of P53-Mdm4. *Chem. Commun.* **2016**, *52*, 5140−5143.
(21) Charoenpattarapreeda, J.; Tan, Y. S.; Iegre, J.; Walsh, S. J.; Fowler, E.; Eapen, R. S.; Wu, Y.; Sore, H. F.; Verma, C. S.; Itzhaki, L.; Spring, D. R. Targeted Covalent Inhibitors of MDM2 Using Electrophile-Bearing Stapled Peptides. *Chem. Commun.* **2019**, *55*, 7914−7917.
(22) Pazgier, M.; Liu, M.; Zou, G.; Yuan, W.; Li, C.; Li, C.; Li, J.; Monbo, J.; Zella, D.; Tarasov, S. G.; Lu, W. Structural Basis for High-Affinity Peptide Inhibition of P53 Interactions with MDM2 and MDMX. *Proc. Natl. Acad. Sci. U. S. A.* **2009**, *106*, 4665−4670.
(23) The reduced modification yield of the Y67F mutant was observed in the labeling reaction *in vitro* and in live HEK293T cells expressing $HDM2_{1-125}$ (Y67F)-HA (Figures S9 and S12). Figure S12 suggests that the contribution of Tyr67 to the reaction would be ∼40% under live cell conditions.
(24) Michelsen, K.; Jordan, J. B.; Lewis, J.; Long, A. M.; Yang, E.; Rew, Y.; Zhou, J.; Yakowec, P.; Schnier, P. D.; Huang, X.; Poppe, L. Ordering of the N-Terminus of Human MDM2 by Small Molecule Inhibitors. *J. Am. Chem. Soc.* **2012**, *134*, 17059−17067.
(25) Hermanson, G. T. *Bioconjugate Techniques*, 3rd ed.; Academic Press, 2013; p 196.
(26) Rosen, C. B.; Francis, M. B. Targeting the N Terminus for Site-Selective Protein Modification. *Nat. Chem. Biol.* **2017**, *13*, 697−705.
(27) Thimaradka, V.; Hoon Oh, J.; Heroven, C.; Radu Aricescu, A.; Yuzaki, M.; Tamura, T.; Hamachi, I. Site-Specific Covalent Labeling of His-Tag Fused Proteins with N-Acyl-N-Alkyl Sulfonamide Reagent. *Bioorg. Med. Chem.* **2021**, *30*, 115947.
(28) Plante, J. P.; Burnley, T.; Malkova, B.; Webb, M. E.; Warriner, S. L.; Edwards, T. A.; Wilson, A. J. Oligobenzamide Proteomimetic Inhibitors of the p53-hDM2 Protein-Protein Interaction. *Chem. Commun.* **2009**, *34*, 5091−5093.
(29) SJSA1 cells have HDM2 gene amplification and are sensitive to Nutlin-based inhibitors: Tovar, C.; et al. MDM2 small-molecule antagonist RG7112 activates p53 signaling and regresses human tumors in preclinical cancer models. *Cancer Res.* **2013**, *73*, 2587−2597.
(30) Chène, P. Inhibiting the P53-MDM2 Interaction: An Important Target for Cancer Therapy. *Nat. Rev. Cancer* **2003**, *3*, 102−109.
(31) Even at the 3 h time point when p53 disappeared, HDM2 and p21 still maintained high expression levels in **1**-treated cells. This might be because these proteins are expressed later than the activation of p53 pathway, rather than simultaneously with it. Chang, L. J.; Eastman, A. Differential Regulation of P21waf1 Protein Half-Life by DNA Damage and Nutlin-3 in P53 Wild-Type Tumors and Its Therapeutic Implications. *Cancer Biol. Ther.* **2012**, *13*, 1047−1057.
(32) Serdjukow, S.; Kink, F.; Steigenberger, B.; Tomás-Gamasa, M.; Carell, T. Synthesis of γ-Labeled Nucleoside 5-Triphosphates Using Click Chemistry. *Chem. Commun.* **2014**, *50*, 1861−1863.
(33) Lanning, B. R.; Whitby, L. R.; Dix, M. M.; Douhan, J.; Gilbert, A. M.; Hett, E. C.; Johnson, T. O.; Joslyn, C.; Kath, J. C.; Niessen, S.; Roberts, L. R.; Schnute, M. E.; Wang, C.; Hulce, J. J.; Wei, B.; Whiteley, L. O.; Hayward, M. M.; Cravatt, B. F. A Road Map to Evaluate the Proteome-Wide Selectivity of Covalent Kinase Inhibitors. *Nat. Chem. Biol.* **2014**, *10*, 760−767.
(34) SJSA1 cells ∼10-fold overexpress HDM2 compared to the other three cell lines (Figure S23).
(35) Tominaga, H.; Ishiyama, M.; Ohseto, F.; Sasamoto, K.; Hamamoto, T.; Suzuki, K.; Watanabe, M. A Water-Soluble Tetrazolium Salt Useful for Colorimetric Cell Viability Assay. *Anal. Commun.* **1999**, *36*, 47−50.
(36) Thress, K. S.; Paweletz, C. P.; Felip, E.; Cho, B. C.; Stetson, D.; Dougherty, B.; Lai, Z.; Markovets, A.; Vivancos, A.; Kuang, Y.; Ercan, D.; Matthews, S. E.; Cantarini, M.; Barrett, J. C.; Jänne, P. A.; Oxnard, G. R. Acquired EGFR C797S Mutation Mediates Resistance to AZD9291 in Non-Small Cell Lung Cancer Harboring EGFR T790M. *Nat. Med.* **2015**, *21*, 560−562.
(37) Chen, W.; Dong, J.; Plate, L.; Mortenson, D. E.; Brighty, G. J.; Li, S.; Liu, Y.; Galmozzi, A.; Lee, P. S.; Hulce, J. J.; Cravatt, B. F.; Saez, E.; Powers, E. T.; Wilson, I. A.; Sharpless, K. B.; Kelly, J. W. Arylfluorosulfates Inactivate Intracellular Lipid Binding Protein(s) through Chemoselective SuFEx Reaction with a Binding Site Tyr Residue. *J. Am. Chem. Soc.* **2016**, *138*, 7353−7364.
(38) Mortenson, D. E.; Brighty, G. J.; Plate, L.; Bare, G.; Chen, W.; Li, S.; Wang, H.; Cravatt, B. F.; Forli, S.; Powers, E. T.; Sharpless, K. B.; Wilson, I. A.; Kelly, J. W. Inverse Drug Discovery" Strategy to Identify Proteins That Are Targeted by Latent Electrophiles As Exemplified by Aryl Fluorosulfates. *J. Am. Chem. Soc.* **2018**, *140*, 200−210.
(39) Hahm, H. S.; Toroitich, E. K.; Borne, A. L.; Brulet, J. W.; Libby, A. H.; Yuan, K.; Ware, T. B.; McCloud, R. L.; Ciancone, A. M.; Hsu, K. L. Global Targeting of Functional Tyrosines Using Sulfur-Triazole Exchange Chemistry. *Nat. Chem. Biol.* **2020**, *16*, 150−159.
(40) Okuda, S.; Watanabe, Y.; Moriya, Y.; Kawano, S.; Yamamoto, T.; Matsumoto, M.; Takami, T.; Kobayashi, D.; Araki, D.; Yoshizawa, A. C.; Tabata, T.; Sugiyama, N.; Goto, S.; Ishihama, Y. jPOSTrepo: an international standard data repository for proteomes. *Nucleic Acids Res.* **2017**, *45*, D1107−D1111.

https://doi.org/10.1021/jacs.1c00703
J. Am. Chem. Soc. 2021, 143, 4766−4774